Analysis of the Accessibility of Macroporous Alumino-Silicate Using 3D-TEM Images

M. Moreaud, B. Celse, F. Tihay.
IFP, B.P. 3 Vernaison, 69390 VERNAISON, FRANCE.

Keywords: 3D-TEM images, images segmentation, porous network, tortuosity.

Abstract

Macroporous alumino-silicate are catalytic materials used in chemical and petroleum industries. Their selectivity and activities are directly linked to the morphology of their texture. By means of 3D transmission electron microscopy (3D-TEM) images, complex information about the structure at the nanometric scale can be obtained. A segmentation method coupled with a method of extraction of the volume of pores keeping intact the irregularity of the surface are presented. Porosity and specific surface area are calculated and compared with classical measures using other physical measurement methods. An analysis of the pore connectivity is presented using a pore-to-pore tortuosity map processed using geodesic constrained distance propagations. It allows a global quantification of the connections between the pores in order to estimate the accessibility to the catalyst for a molecule of a known size.

Introduction

The increasing level of research for nanoparticles and nanostructured materials performed on the nanometric scale requires powerful tools to characterize objects. In particular, in chemical or petroleum industries, researchers face the difficulty to precisely known the results of interaction between catalytic particles and the porous structure of their support. The selectivity and activities of catalysts materials is directly linked to the morphology of their texture. The recent development achieved in transmission electron microscopy (TEM) with automation of signal acquisition allows new characterization capabilities of nanomaterials by means of tomographic techniques. With the obtained 3D transmission electron microscopy (3D-TEM) images, complex information about the morphology at the nanometric scale can be performed [1]. A specific analysis of such 3D images allows the quantification of the volume and the specific surface area of the pores. Such data are extremely important for catalytic cracking of heavy crude oil, because one must be able to predict if a heavy molecule can enter or not inside the grain of catalysts before cracking. This kind of questions will be more and more a hot topic, as the price of the barrel rises, and the quality of the oil decreases. In the paper, we focus on the analysis of macroporous alumino-silicate catalysts by means of 3D-TEM images. Three samples of this material are analyzed. An efficient method of pre-filtering and segmentation of the 3D images is presented. A technique to extract the porous network is also explained. Measurement of the porosity and of the specific surface area are achieved and compared to other physical measurement methods to validate both segmentation and extraction techniques. Also a specific analysis is performed in order to obtain information about the accessibility to the pores for a molecule of a known diameter.

Acquisition of 3D-TEM images of macroporous alumino-silicate

Macroporous alumino-silicate catalysts are obtained by aerosol synthesis [2] made of spherical macroporous and mesoporous particles, with microporous alumino-silicate walls. The diameter of these particles is about 200 nm to 2 µm. Three samples of these material are studied using 3D-TEM images. The acquisition of 3D-TEM images is achieved in several steps:

- automatic TEM bright field images acquisition of series of projections of the materials (Fig. 1).
- semi-automatic alignment of projections by cross-correlation technique and particles tracking technique.
- tomographic reconstruction by filtered retroprojection technique.

3D images of the samples are obtained with a resolution of 0.5 nanometer by voxel (within the three axis) (Fig. 1). For practical purposes (essentially for memory and time processing limitations), in the following, sub-sampled images are used for the proposed image processing and analysis.

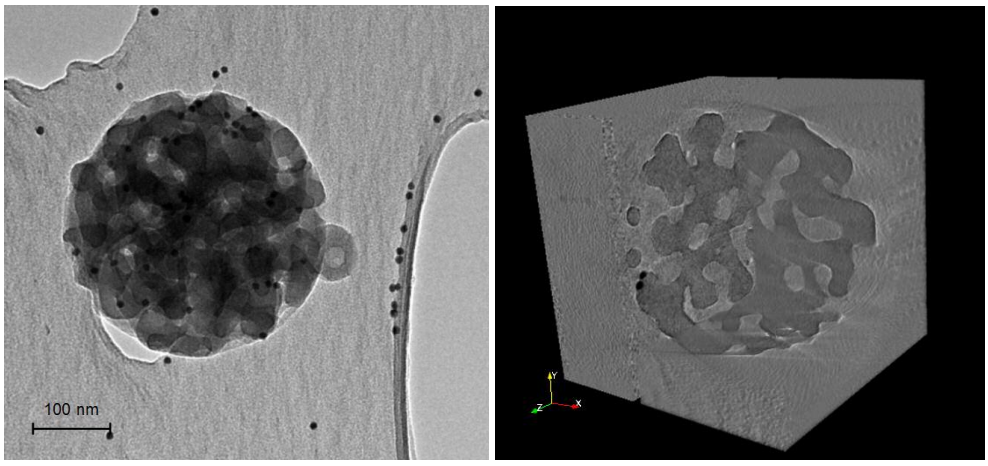

Figure 1. Left, 2D-TEM projection image of a typical porous alumino-silicate (0.5nm / voxel). Right, crop of its 3D-TEM reconstruction image (1.7nm / voxel).

Automatic segmentation of the 3D-TEM images

Pre-filtering for noise and artifacts reduction

A correct segmentation between the material and the outside must be achieved in order to analyse the porous network of the macroporous alumino-silicate samples. To remove the noise and to smooth the artefacts due to the tomographic reconstruction, a first step of pre-filtering should be performed. Two methods of pre-filtering are been compared.

The first one, is an anisotropic diffusion filter [3]. This kind of filter is commonly use in medical images for preserving edges and reducing noise and texture. Mathematically anisotropic diffusion is formulated as:

$$\frac{\partial g(x,y,z,t)}{\partial t} = \nabla . c\left(\left\|\nabla g\left(x,y,z,t\right)\right\|\right)\nabla g\left(x,y,z,t\right)$$

where g is the image, t refers to the iteration step and c is a diffusion function (monotonically decreasing function of the image gradient magnitude). A very common choice for c is $c(\nabla g) = e^{-\left(\frac{\|\nabla g(x,y,z)\|}{K}\right)^2}$, where K is a conductance parameter, which controls the sensitivity of the process to edge contrast. Typical values of parameters are given by Insight Segmentation and Registration Toolkit (ITK) consortium [4] in the case of 3D data smoothing : 10 iterations, t=0.0625 and K=3.

The second method of pre-filtering that we compared is a bilateral filter [5] with a specific implementation. The bilateral filter is a nonlinear and non iterative filter which smooth a signal while preserving strong edges. It derives from a blur filter but it prevents blurring accross edges by decreasing the weight of pixels when the intensity difference is too large. The output O of the bilateral filter for an image I with spatial support D and a pixel x is given by:

$$O(x) = \frac{1}{k(x)} \sum_{y \in D} f(x-y) g(I(x) - I(y)) I(x)$$

where k(x) is a normalization term: $k(x) = \sum_{y \in D} f(x-y) g(I(x) - I(y))$

Several edge-stopping functions can be used for f and g such like Gaussian functions, or Tukey's biweight function for instance. In our case, best results are obtained using this last one with parameters σ=3 and 20 for f and g respectively :

$$f(x) = g(x) = \begin{cases} \frac{1}{2}\left[1 - \left(\frac{x}{\sigma}\right)^2\right]^2 & |x| \le \sigma \\ 0 & otherwise \end{cases}$$

In the literature, several fast implementation of this filter are proposed [6] [7]. We choose to implement a non exact formulation of the filter with low memory consuming and fast computation. We linearize the filter and use direct convolution [8] .

For memory and time consuming purpose, we chose to use the bileral filter with the specific mentioned implementation. The results are still accurate compared to these obtained with an anisotropic diffusion filter. (Fig. 2).

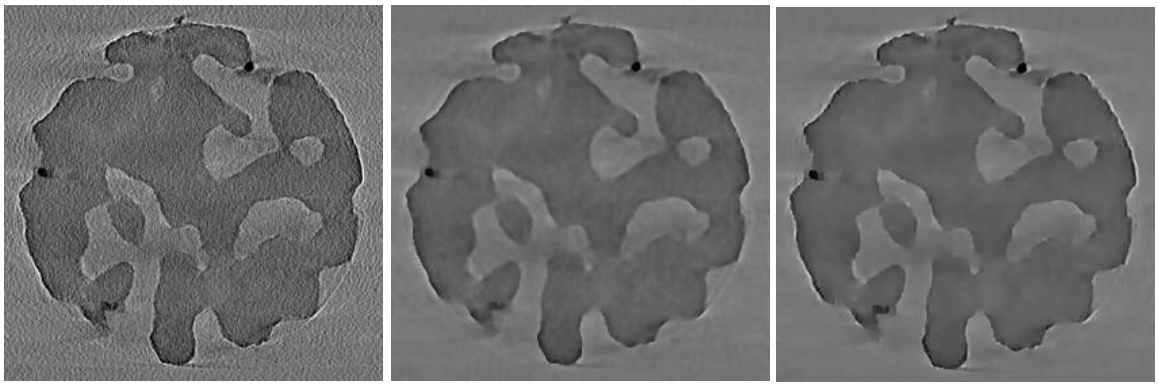

Figure 2. Planar cut of the 3D-TEM image of a porous alumino-silicate (1.7nm / voxel). Left to right: initial image; image after anisotropic diffusion filtering; image after bilateral filtering.

Segmentation of the material

After this pre-filtering, the inside of the material appears globally with dark grey voxels, while the outside appears with light grey voxels. Unfortunately these two sets are not homogenous, so a segmentation only based on the analysis of the histogram is not sufficient. We propose an automatic segmentation with two steps. The first step is based on an analysis of the histogram to determine approximately the markers of the two sets. The second step consists in completing the segmentation by means of a propagation of the markers using a watershed operator [9].

In the first step, the histogram *histo(t)*, $t \in [0,M]$ of the initial 3D-TEM image *IniMat* is segmented in order to obtain markers. We use the fact that a fraction f_{in} of the darkest voxels belongs surely to the material, and that a fraction f_{out} of the lightest voxels belongs surely to the outside. A threshold thr_{MIV} separating approximately the material and the outside is obtained by an automatic method using maximization of the interclass variance [10]. Two types of markers can be defined for the material $Mark_{in}$ and for the outside $Mark_{out}$ on the image *IniMat*(p) with spatial support D (Fig. 3) :

$$Mark_{in} = \bigcup_D p \,|\, IniMat(p) < thr_{in}$$

$$\text{where } thr_{in} = \max_{t \in [0,M]} t \left| \sum_{i=0}^{t} histo(i) \le f_{in} . \sum_{j=0}^{thr_{MIV}} histo(j) \right.$$

$$Mark_{out} = \bigcup_D p \,|\, IniMat(p) > thr_{out}$$

$$\text{where } thr_{out} = \min_{t \in [0,M]} t \left| \sum_{i=0}^{t} histo(i) \ge \sum_{j=0}^{M} histo(j) - f_{out} . \sum_{k=thr_{MIV}}^{M} histo(k) \right.$$

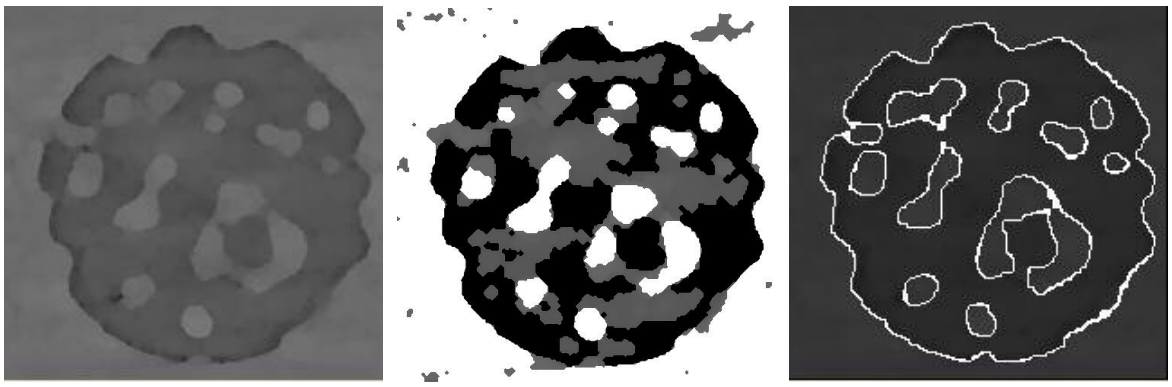

Figure 3. Planar cut of the 3D-TEM image of a porous alumino-silicate (1.7 nm / voxel). From left to right : initial filtered image; markers $Mark_{in}$ (in black) $Mark_{out}$ (in white) for $f_{in} = f_{out} = 0.6$; result of the watershed segmentation of the material.

In the second step, the segmentation is completed by propagating the markers using a unbiased watershed operator [9] on the contour image of the initial image (Fig. 3). This image is

interpreted as a topographic relief where the contours correspond to crest lines of the relief. The topographic relief is then flooded starting for the markers considered as minima. The watershed lines are the meeting line of two flooding fronts coming from two distinct minima.

An accurate image of the contours is computed by applying a first derivative Gaussian filter with σ=2 [11][12]. We obtain an image of the segmented material *SegMat*:

$$SegMat = \text{watershed}(GaussFirstDer(IniMat, \sigma=2), Mark_{in} \cup Mark_{out})$$

At this stage, an accurate segmentation of the material is obtained (Fig. 4).

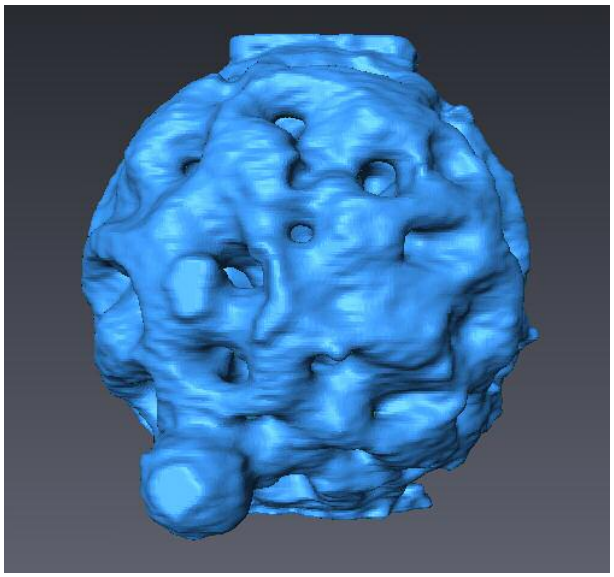

Fig. 4. Segmentation of a 3D-TEM image of the material.

Extraction of the porous volume

To extract the porous network, we propose to fill the pores inside the material by means of an approach using morphological mathematic tools. First, the maximum diameter *maxdiam* of the pores has to be calculated:

• An estimation of the convex envelop *ConvEnv* of the material *SegMat* is necessary. For instance, we can compute it by means of a morphological close of infinite size (in practical, the size of the close is chosen higher than the maximum diameter of all the pores).

$$ConvEnv = \varphi_{\infty}(SegMat)$$

• A geodesic constrained distance d [13] [14] is propagated from the material within the outside. We obtain an image *DistOut:*

$$DistOut = d_{SegMat^c}(SegMat)$$

where $SegMat^c$ is the complementary image of *SegMat*.

• An approximation of the maximum diameter *maxdiam* of the pores is given by the maximum of the distance inside the convex envelop.

$$maxdiam = \max\left\{DistOut(p) \middle| p \in ConvEnv\right\}$$

The value *maxdiam* is then used in morphological geodesic operations [15] in order to extract the porous volume. The morphological geodesic dilation and erosion of size n of a set X within the set Y are given by respectively :

$$\delta_X^{(n)}(Y) = \left\{p \in X, d_X(p,Y) \le n\right\}$$
$$\varepsilon_X^{(n)}(Y) = \left\{p \in X, d_X(p,Y^c) \ge n\right\}$$

where Y^c is the complementary image of Y.

The extraction is then performed in three steps:

• To surely fill all the pores of the material, we perform a morphological geodesic dilation of size *maxdiam* of the segmented material *SegMat* within the outside $SegMat^c$. We obtain a new image *DilSegMat.*

$$DilSegMat = \delta_{SegMat^C}^{(maxdiam)}(SegMat)$$

At this stage, all the pores of the initial material are filled.

• To completely restore the external irregularity on the external surface of the material, we achieve a morphological geodesic erosion of size *k.maxdiam* of *DilSegMat* within the outside $SegMat^c$. The value of *k* should be chosen greater than the maximum between one and the height $h_{Sirrmax}$ equals to the highest irregularity on the surface of the material. In practical, an estimation of this irregularity is difficult, and *k* is taken equals to 2. By this way, *w*e obtain a new image *EroDilSegMat*.

$$EroDilSegMat = \varepsilon_{SegMat^C}^{(k.maxdiam)}(DilSegMat)$$

By taking *k.maxdiam* with $k>\max(1,h_{Sirrmax})$, the surface irregularity of the material is totally recovered, but the volume of pores is underestimated.

• The porous volume is finally obtained by a morphological geodesic dilation of size *(k-1).maxdiam* of *EroDilSegMat* within the outside of the material $SegMat^c$. We obtain a new image *PorousVol* :

$$PorousVol = \delta_{SegMat^C}^{((k-1).maxdiam)}(EroDilSegMat)$$

With this final operation, the porous volume *PorousVol* is extracted without filling the irregularity on the surface of the material.

At the end of these three steps, an accurate estimation of the internal porous volume of the material is obtained keeping intact the surface irregularity (Fig. 5). Also, the external surface $Surf_{ExtPore}$ of emerged pores can be obtained by taking the intersection between the porous volume *PorousVol* and the complementary of the filled volume *FillVol* dilated by a ball of radius one. *FillVol* is the union between the material and the extracted porous volume.

$$FillVol = PorousVol \cup SegMat$$

$$Surf_{ExtPore} = (PorousVol \cap \delta_1(FillVol^c))$$

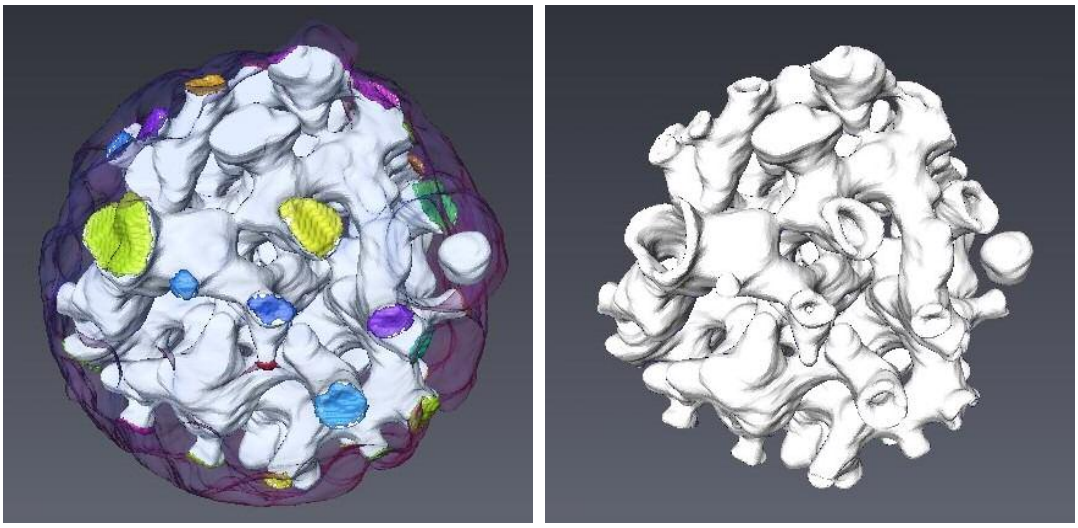

Fig. 5. Left: initial material (SegMat) and by transparency the inside porous network (PorousVol). In color, external surface of emerged pores ($Surf_{ExtPore}$). Right: Extracted porous network of the material (PorousVol).

Estimation of the macro porosity and of the specific surface area using image analysis

We compare some measurements performed by image analysis with physical ones to validate both methods of segmentation and extraction of the porous network. The volume can be estimated by counting the number of voxels of the image *PorousVol*. By taking a density of 1.2 $g.cm^{-3}$, which is the value of a classical microporous alumino-silicate, an estimation of 0.337 $cm^3.g^{-1}$ for the macro porosity is obtained (Tab. 1). This value can be compared to nitrogen adsorption measurements estimated to 0.22 $cm^3.g^{-1}$±0.05 $cm^3.g^{-1}$. This result is suitable with our results obtained by automatic image analysis. If we do not consider the result obtained with the lowest resolution volume (sample 3) witch is the most imprecise one, the results for the other volumes are very close to the physical measurement method (Tab. 1).

An estimation of the specific surface area of the macro-porosity can be achieved by means of an estimation of the surface area of the porous volume within the material. This area can be estimated using the image *PorousVol* and the image $Surf_{ExtPore}$:

$$\text{Area}(PorousVol) - \text{Area}(Surf_{ExtPore})$$

where $Surf_{ExtPore}$ is the external surface of the emerged pores (calculation explained previously).

To compute this area directly on the discrete volume composed by voxels, a surface area estimation by weighted local configurations is used [16]. Other similar method can also be used [17]. We obtain an estimation of 30 $m^2.g^{-1}$ (Tab. 1). This result can be compared to classical physical techniques such as nitrogen adsorption measurement, coupled to mercury porosity, which gives a surface area of 31 $m^2.g^{-1}$ for the macro porosity. This result is very close to our result achieved using automatic image analysis.

Table 1 Macro porosity and specific surface area of the three samples of macroporous alumino-silicate.

Sample	Resolution (nm/voxel)	Porosity (cm^3/g)	Specific surface area (m^2/g)
1	2.24	0.299	28.4
2	1.68	0.238	24.4
3	7.18	0.474	37.3
Average		**0.337**	**30**

Accessibility to the porous network

Information about the connectivity of the pores can be achieved by the study of the porous volume. The method of analysis that we present further to estimate the accessibility from a pore to one other for a molecule of a known size. With this kind of data, we can predict if a heavy molecule can or not enter and exit inside the grain of catalyst. To obtain this information, we build a pore-to-pore tortuosity map. A similar approach is used in [18] with the calculation of a pore-to-pore distance map.

The pore-to-pore tortuosity map is given by the ratio between geodesic and Euclidean distance between two external surfaces of the emerged pores. The binary image of the external surfaces of the pores $Surf_{ExtPore}$ obtained previously have to be labelized in connected components in order to identify each emerged pores. The Euclidean distance $distEuc_{pi\text{-}pj}$ between two pores p_i and p_j can be estimated by the distance between the barycenters b_{pi} and b_{pj} of their emerged surface $Surf_{ExtPore}^{pi}$ and $Surf_{ExtPore}^{pj}$.

The geodesic distance distGeo is obtained as follows. We calculate the 3D skeleton *SqP* of the porous network by means of 3D curve thinning method [19].

$$SkP = \text{3DThinning}(PorousVol)$$

This binary skeleton can be valuated by the corresponding local section diameter of the pores obtained by taking the value of the skeleton by ultimate erosion UEskeleton [20] of *PorousVol* dilated by a sphere of diameter equals to *maxdiam* (the maximum diameter of the pores, estimated in a previous section). This local section diameter corresponds to the maximum ball that can be contained locally in the pores.

$$SkP = \delta^{maxdiam}(\text{UEskeleton}(PorousVol)) \,|\, p \in SkP$$

To surely connect the skeleton of the porous network *SkP* to the external surface of emerged pores, we take the union between *SkP* and the geodesic dilation of size *maxdiam* of $Surf_{ExtPore}$ in *PorousVol.*

$$SkP = \delta_{PorousVol}^{maxdiam}(Surf_{ExtPore}) \cup SkP$$

Illustrations of the calculated skeleton for the sample 2 is showed in figure 6.

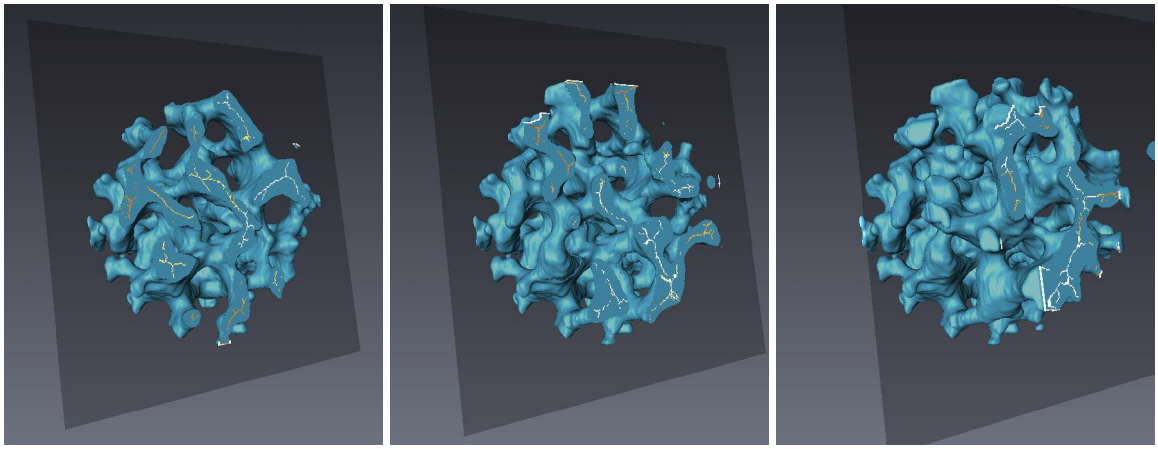

Fig. 6. Skeleton of the porous network (SkP) of the sample 2 for different planar cuts.

Now, we can propagate for each emerged pores p_i identified by its emerged surface $Surf_{ExtPore}^{pi}$, a geodesic constrained distance from $Surf_{ExtPore}^{pi}$ within the skeleton of the porous network to obtain $Dist_{pi}$.

$$Dist_{pi}=d_{SkP}(Surf_{ExtPore}^{pi})$$

The distance $distGeo_{pi\text{-}pj}$ from the pore p_i to one other pores p_j is achieved by taking the average distance observed on the emerged surface $Surf_{ExtPore}^{pj}$ of the pore p_j:

$$distGeo_{pi\text{-}pj} = \overline{Dist}_{pi}(p) \mid p \in Surf_{ExtPore}^{pj}$$

where $\overline{Dist}_{pi}(p)$ is the average value of the image $Dist_{pi}$ calculated on points p.

The pore-to-pore tortuosity map is then obtained by the ratio between $distEuc_{pi\text{-}pj}$ and $distGeo_{pi\text{-}pj}$ for all possible combinations of p_i-p_j. The deletion of points p of *SkP* equals to a value s, is equivalent to fill all the pores of minimum section diameter s. By iteration of the given procedure with different value of s, we obtain the accessibility pore-to-pore tortuosity map for molecules with diameter inferior or equals to s. Such a map can be visualized by means of a 2D histogram with values corresponding to the pore-to-pore tortuosity (Fig. 7). A pore-to-pore maximum size molecule accessibility map can be calculated by taking, for each pore-to-pore connection, the maximum diameter before the cutting of this connection (Fig. 8). A characterization of the accessibility to a catalyst can be performed by the calculation of the percentage of the interconnections between pores where molecules of a given diameter can go thought the entire material (i.e. can enter by a pore and exit by one other) (Fig. 9). We can notice that for the 3 samples, 100% of the interconnections between pores can be crossed by molecules with a maximum diameter of approximately 5 nm (asphaltenes for instanceà. For the samples 1 and 2, 50% of these interconnections can be still crossed by molecules with a maximum diameter of approximately 12nm. For the sample 3, the same result is obtained by molecules with a maximum diameter of approximately 17nm. Such analysis give us precise knowledge about the activity of the these catalysts, and the type of products on which it could be active.

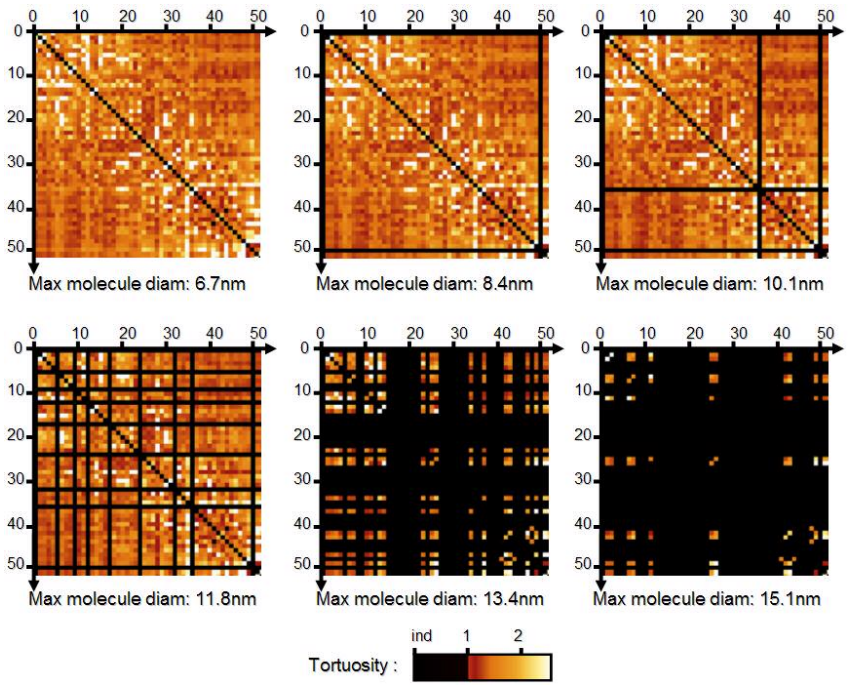

Fig. 7. Pore-to-pore tortuosity maps for given sizes of molecules for sample 2. The axis correspond to the label of pores. Black points correspond to indefinite tortuosity (the geodesic distance between the two pores is infinite, the connection between the two pores is cut).

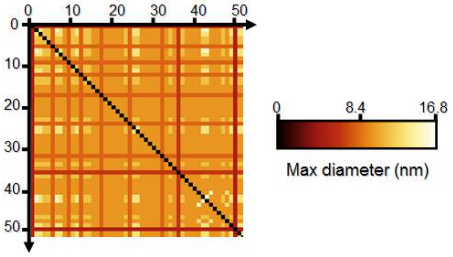

Fig. 8. Pore-to-pore maximum size molecule accessibility map for the sample 2. The axis correspond to the label of pores. Each point (i,j) corresponds to the maximum size of molecules that can go from the pore i to the pore j.

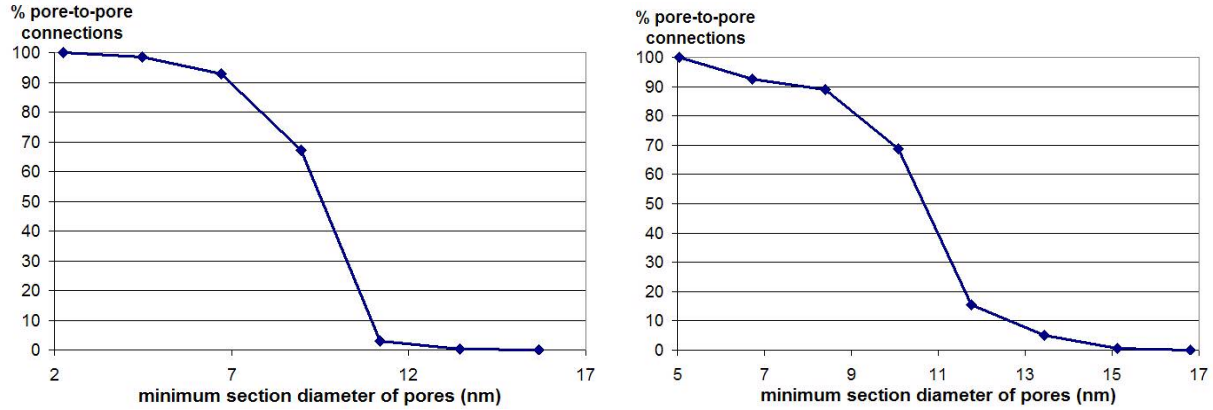

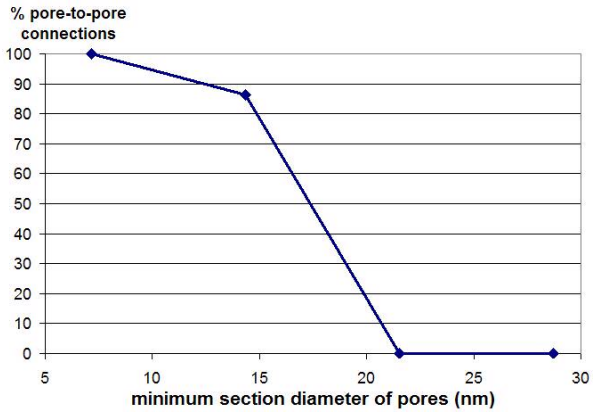

Fig. 9. Percentage of pores interconnections where molecules of a given diameter can go thought the entire material. Top left: sample 1. Top right: sample 2. Down: sample 3.

Conclusions

In this paper, we present an application of segmentation techniques for 3D-TEM images of macroporous alumino-silicate. This material is an efficient catalytic material used in petroleum industries. A method for an automatic extraction of the porous network keeping intact the surface irregularity is proposed. The accuracy of the methods for both segmentation and estimation of the porous volume is validated by comparison of measurements of the porosity and of the specific surface area between image analysis and global physical methods. An analysis of the porous network by means of a pore-to-pore tortuosity map is also presented. Such analysis give information about availabilities for molecules of a given diameter to cross the material.

References

[1] O. Ersen, C. Hirlimann, M. Drillon, J. Werckmann, F. Tihay, C. Phamm-Huu, C. Crusifix, P. Schultz, 3D-TEM characterization of nanometric objects, *Solid State Sciences* 9 (2007), 1088-1098.

[2] S. Areva, C. Boissière, D. Grosso, T. Asakawa, C. Sanchez, M. Linden, *Chem. Commun.* (2004) 1630-1631.

[3] P. Perona and J. Malik. Scale-space and edge detection using anisotropic diffusion, *IEEE Transactions on Pattern Analysis Machine Intelligence*, 12 (1990), 629–639.

[4] L. Ibanez, W. Schroeder, L. Ng, and J. Cates. The ITK Software Guide. Kitware, Inc., second edition (2005).

[5] C. Tomasi, R. Manduchi, Bilateral filtering for gray and color images, *Proc. of International Conference on Computer Vision, IEEE* (1998), 839-846.

[6] S. Paris, F. Durand, A Fast Approximation of the Bilateral Filter using a Signal Processing Approach, *European Conference on Computer Vision* (ECCV'06) (2006).

[7] F. Durand, J. Dorsey, Fast Bilateral Filtering for the Display of High Dynamic-Range Images, *ACM Siggraph* (2002).

[8] T.Q. Pham, L.J. van Vliet, Separable bilateral filtering for fast video preprocessing, *International Conference on Multimedia and Expo, IEEE* (2005).

[9] S. Beucher, Unbiased Implementation of the Watershed Transformation based on Hierarchical Queues. *CMM Internal note, Paris School of Mines* (2004).

[10] N. Otsu, A Threshold Selection Method from Grey-Level Histograms, *IEEE Trans. Systems, Man, and Cybernetics*, vol. 9, no. 1 (1979), 377-393.

[11] R. Deriche, Recursively implementing the Gaussian and its derivatives, *Technical Report 1893, INRIA* (1993).

[12] G. Farneback, C.F. Westin, Improving Deriche-style Recursive Gaussian Filters, *Journal of Mathematical Imaging and Vision*, volume 26, Issue 3, (2006), 293-299.

[13] P. Soille, Morphological Image Processing: Principles and Applications (second ed.), Springer-Verlag (2003).

[14] L. Vincent, New trends in morphological algorithms, *Proceedings of SPIE/SPSE*, vol. 1451 (1991), 158–170.

[15] C. Lantuéjoul, F. Maisonneuve, Geodesic methods in quantitative image analysis. *Pattern recognition*, 17(2), (1984), 177-187.

[16] J. Lindblad, Surface area estimation of digitized 3D objects using weighted local configurations, Image and Vision Computing 23 (2005), 111-122.

[17] G. Windreich, N. Kiryati, G. Lohmann, Voxel-based surface area estimation : from theory to practice, Pattern Recognition 36 (2003), 2531-2541.

[18] G. Van Dallen, P. Nootenboom, L.J. Van Vliet, L. Voortman, E. Esveld, 3-D imaging, analysis and modeling of porous cereal products using X-ray microtomography, *Image Anal Stereol* 26 (2007), 169-177.

[19] C. Lohou, G. Bertrand, A 3D 6-subiteration curve thinning algorithm based on P-simple points, *Discrete Applied Mathematics* 151 (2001), 198-228.

[20] J. Serra, Image Analysis and Mathematical Morphology - Vol. I, Ac. Press, London (1982).